Int. J. Simul. Multidisci. Des. Optim. **13**, 21 (2022)

https://doi.org/10.1051/smdo/2022014

IJSMDO
Available online at:
https://www.ijsmdo.org

Advances in Modeling and Optimization of Manufacturing Processes

RESEARCH ARTICLE OPEN ACCESS

Optimization of the Young's modulus of woven composite material made by *Raphia vinifiera* fiber/epoxy

Alfred Kendem Djoumessi[1,2,3,*], Rodrigue Nicodème Sikame Tagne[1,2,3,*], Tido Tiwa Stanislas[3], François Ngapgue[1,2,3], and Ebenezer Njeugna[3]

[1] Research Unit for Mechanics and Modeling of Physical Systems- (UR2MSP), University of Dschang, Cameroon
[2] Research Unit of Industrial and systems Engineering Environment (URISIE), University Institute of Technology (FOSTO Victor Bandjoun), University of Dschang, Cameroon
[3] Laboratory of Mechanics and Adapted Materials (LAMMA), ENSET, University of Douala, Cameroon

Received: 10 December 2021 / Accepted: 20 September 2022

Abstract. This work focuses on the optimal design of the woven fabrics made from *Raphia vinifiera*, fiber, and their contribution as reinforcing element in the epoxy matrix. The work is done alternately experimentally and theoretically. The woven made of canvas, twill and satin armor are characterized in traction according to the ISO13934-1 standard [1]. A predictive mathematical model of Young's modulus of the woven with the greatest rigidity is established. The woven reinforcement composite made is characterized in traction and bending according to EN ISO 527-5 [2] and NF EN ISO 14125 [3] standards. In order to determine the reinforcement rate which gives the highest young modulus of the material, the gradient method was applied on some prediction equations of Young's modulus of composite material. Then find the prediction equation that best corresponds to the composite made. The results showed that mathematical modeling works corroborates with experimental works. On the woven fabrics the canvas armor has the highest Young's modulus in the warp and weft direction (2.429, 21.164 GPa). Followed by twill (2315, 18 741 GPa) and satin (2184, 18.54 GPa). On the composite, the reinforcement rate from which the material is optimized is 50%. The composite young's moduli in the warp and weft direction resulting from the tensile and bending tests of the composite are respectively (3.644, 7.31 GPa) and (1.802, 4.52). In a nutshell, this work presents the theoretical and experimental aspect of the best material which can be obtained with *R. vinifiera* fiber with respect to its Young modulus.

Keywords: Optimization / woven / modeling / Young modulus

1 Introduction

The use of composites with woven reinforcements of natural fibers is increasingly prominent in various fields of activity, given the growing concern about environmental issues and the need to find a realistic alternative to non-biodegradable materials [4]. Researchers are now interested in the implementation of bio-composite materials with plant fibers as reinforcements. As a result, mineral and synthetic fibers are replaced by long plant fibers [5] and short plant fibers [6] for the implementation of bio-composites. From then on, the search for the material with optimal rigidity becomes a perpetual watch in the design of bio-composites. For their rigidity, woven reinforcement composite materials have proven to be more effective [7]. From the waves, the best architecture is the unidirectional followed by the bidirectional [8]. The reinforcement of the material in both directions by weaving solves the delamination problem posed by the juxtaposition of conventional laminated layers reinforced in a single direction [9]. The search for the optimal bidirectional woven reinforcement armor between canvas, twill and satin is the first objective of this work. The characterization in tensile test the woven samples according to the three armors in order to compare their young's modulus. The second objective is to propose a prediction equation to obtain the young's modulus of the woven according to that of the fiber and its geometry. Since most research work on the modelization of the tensile behavior of textile structures permit to determine only the deformation of the woven according to the load applied to it, some researchers recently attempted to develop a mathematic model to predict the mechanical properties of the textile fibers such as [10]. Much of this modeling work is based on the research of [11] which brings together empirical work on geometric modeling of textile structures. The complexity of these

* e-mails: kendjoums@gmail.com; nicodeme.sikame@univ-dschang.org

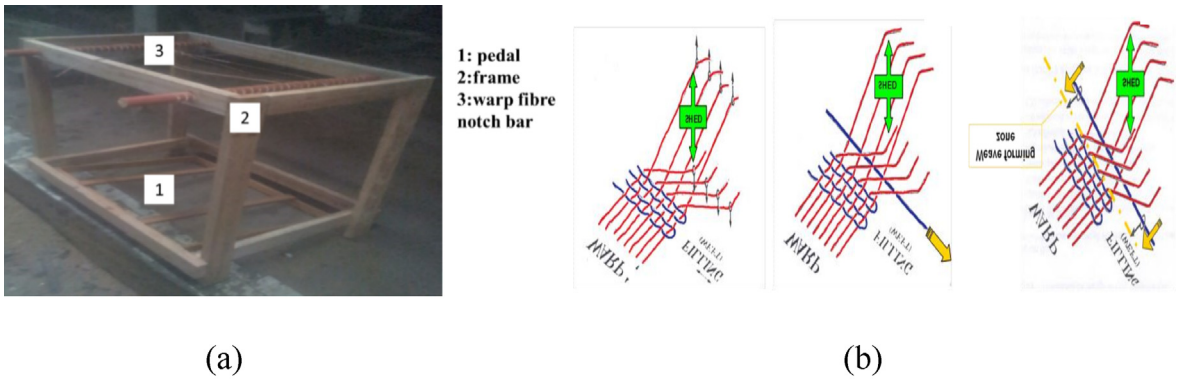

Fig. 1. Development of woven fabrics (a) craft loom, (b) weaving method [12]. The mass and warp and weft count averages of the 25 woven samples by armor and weave direction used are shown in Table 1.

models has led to the development of several software for solving the equations arising from various models. For example, TEXGEN used by [13] to model and simulate in traction composites with complex reinforcement structures and WISETEX used by [14] to model and simulate composites made of canvas, twill and satin armor. Having determined the optimal reinforcement structure, the bio-composite is made with raffia fiber used for its specific resistance [15] and epoxy resin due to its best mechanical properties among resins [16]. Although the use of bio-composite remains restricted to coating and filling applications, they should have high performance, be of quality, be reproducible, durable, reliable and subject to the standards of their fields of applications [17]. Hence, the need to optimize their performance. Optimization work has been done by the authors such as [18], on thermal comfort and UV protection of knits [19]; on optimizing the performance of agave fiber to facilitate its adhesion with the matrix [20]; on optimizing the physicochemical parameters of a composite to reinforcement woven by the neural network. In addition, the work on the effect of the chemical treatment of raffia fibers will vinify in the rigidity of the composite where it reinforces the polyester resin [21], lead us to seek the levels of volume reinforcement of woven fiber that can permit to obtain a composite whose young's modulus is as large as possible. The volume ratio of reinforcement allowing to have the largest Young's modulus can be obtained by the Taguchi method [22] or by mathematical equation. Several equations for modeling the behavior of composites can predict its Young's modulus as a function of the properties of its constituents and the rate of reinforcement. The law of mixtures is one of the oldest. Several models have been developed following it, such as the Chamis model for the evaluation of the transverse Young's modulus and that of Hopkins which takes into account the fiber matrix interface problems [23] and that of Osoka which takes into account the interphase problems, the architecture and the nature of the reinforcement [24]. The last objective of this work is to determine the proportions of reinforcements and resin giving the material optimum rigidity and to determine the model which best corresponds to the composite produced. To achieve the last objective, the gradient optimization method is applied to the young's modulus prediction equations of composites. And finally, it will develop and characterize in tensile then in bending the composites in order to compare the theoretical and experimental results.

2 Materials and methods

2.1 Experimental approach

2.1.1 Fiber procurement

The fibers used come from the stems of the *Raphia vinifiera* harvested in the village Baleveng in west Cameroon. Once the raffia is harvested, it is extracted from its stem (petiole) the shell and directly the fibers are removed manually. This guarantees the best mechanical properties of the fiber as shown [25] (number of sampling areas developed by [15] are not taken into account. To evaluate the impact of the Young's modulus of the fiber on that of the woven, this will be taken into account during the modeling work to obtain all possible values of Young's modules of the woven. And for composite modeling, it is the average Young's modulus of the fiber that was used 4.4 GPa [15].

2.1.2 Obtaining the fabric

The fibers obtained are classified in the craft loom in the warp direction and the weaving is done manually from one fiber to another according to the desired armor in the weft direction. Figure 1 shows the craft loom to be used and schematics of the weaving method.

The images of the different weaves made and the drawing of their graphic representation are presented in Figure 2.

2.1.3 Composite development

The method of elaboration of the composite used is the contact method for its simplicity of implementation and its inexpensive cost. The resin used is epoxy due to its highest young's module. The young modulus (E_m) is 3.1 GPa in traction and 2.9 GPa in bending [27].

2.2 Mechanical tests

The tensile and bending tests were carried out on a test machine type M.O. As this machine is not equipped with a data acquirer, the principle of counting consists in recording

Table 1. Mean geometric characteristic of woven reinforcement samples.

Plain		Twill of 2–2		Satin of 8–8		
Weft	Chain	Weft	Chain	Weft	Chain	
Mass (g)	21.22 ± 5%		18.61 ± 5%		20.6 ± 5 %	
Count (fiber/cm)	6	2	6	2	6	2

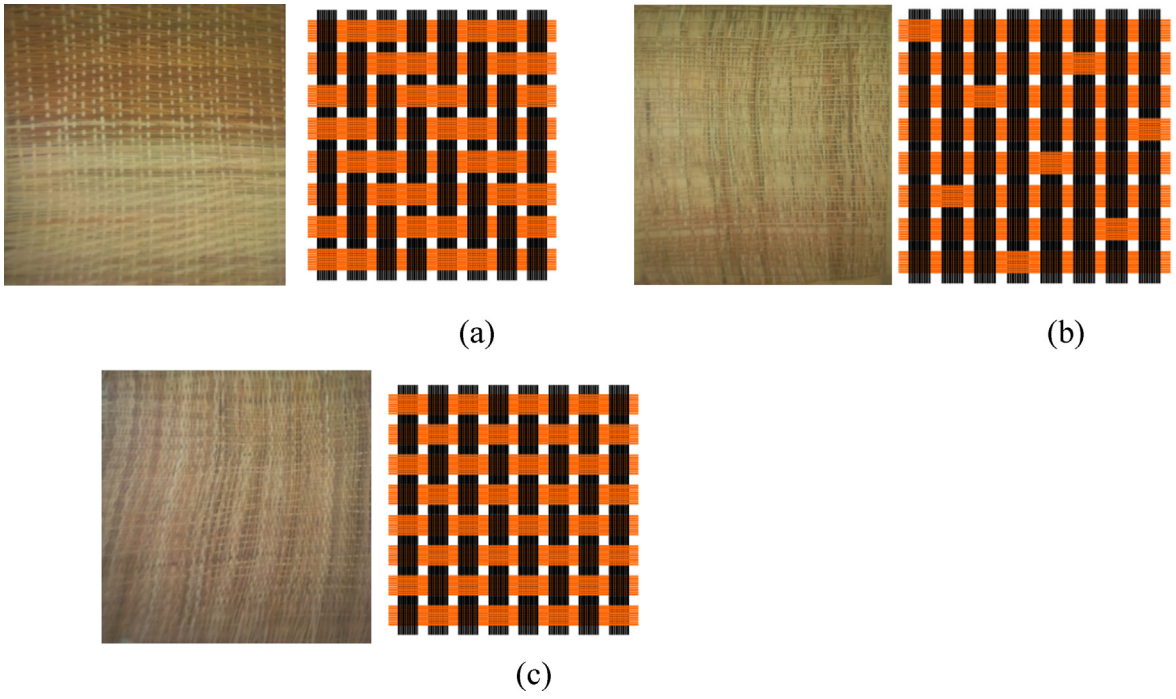

Fig. 2. Image of woven armor and the representation of a weaving sequence: (a) twill 2–2, (b) satin 8–8 and (c) canvas [26].

the values displayed on the comparators in video. These videos are then converted to images in the EM Total Video Converter – HD version 3.71 (Registered) software at a rate of 10 frames/s. This method of data analysis and processing is presented by [28]. Tensile tests are carried out according to ISO 13934-1 for woven fabrics and EN ISO 527-5 for composite. The three-points bending test is carried out according to NF EN ISO 14125. The standards used specify the conditions to be met to carry out the various tests (sample dimensions, cutting condition, test speed, etc.).

2.2.1 The tensile test

The analysis of the figures of the test is done methodically. The force (F) is giving by multiplying the elongation (Δx) of the ring by its stiffness (K). Defined in equation (1):

$$F = K\Delta x. \tag{1}$$

The constraint (σ) of the stress curve strain is obtained by the equation (2):

$$\sigma = \frac{F}{bt}, \tag{2}$$

where b the t represent the width and thickness of the sample.

Deformation is obtained by dividing the elongation by the initial length L_0,

$$\varepsilon = \frac{(\Delta x)}{L_0}. \tag{3}$$

Young's modulus (E) given by the equation (4) correspond to the slope of the experimental stress deformation curve.

$$E = \frac{\Delta F \cdot L_0}{b \cdot t \cdot \Delta L}. \tag{4}$$

The device of the tensile test is shown in Figure 3.

2.2.2 The bending test

The tree-points bending test is done according to adaptation for standards about laminate of machine test. The young modulus (E) and stress (σ) are respectively given by equations (5) and (6) used by [29] for a hemp-epoxy woven reinforcement composite.

$$E = \frac{\Delta F L^3}{4 \cdot b \cdot d^3 \Delta f}, \tag{5}$$

(a)

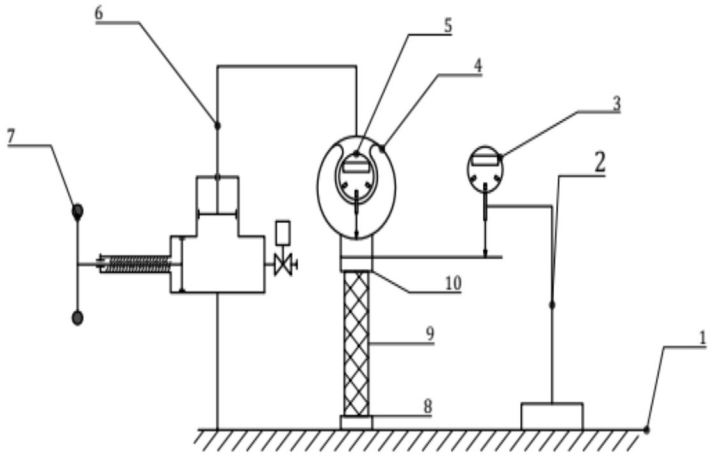

Nomenclature:

1- Frame
2- Lever support
3- Numeric comparator
4- Elastic ring
5- Numeric comparator
6- String stem
7- Lever
8- Lower bit
9- Sample
10- Upper bit

(b)

Fig. 3. Machine used for the tensile test: (a) image for the tension machine, (b) principle scheme of machine.

and

$$\sigma = \frac{3\Delta F L}{2bd^2}, \tag{6}$$

where b, d are respectively the width and thickness of the sample. And, L is the distance between supports in bending three points tests.

The experimental device for the bending test according to the measurement of the displacement (Δf) due to the effect of a variable ΔF load on the sample. The measured loads and displacements make it possible to draw the experimental line (force, displacement). Once the line is drawn, the ratio of force on the displacement (the slope K)

$$K = \frac{\Delta F}{\Delta f}, \tag{7}$$

is multiplied by the quadratic moment (constant A),

$$A = \frac{L^3}{4 \cdot b \cdot d^3}, \tag{8}$$

to get Young' s modulus

$$E = AK. \tag{9}$$

Figure 4 shows the device of the three-points bending test.

2.3 Theoretical approach

2.3.1 Geometric modeling of woven

This modeling aims to determine the young's modulus of the canvas armor woven according to the geometric and mechanical characteristics of the fiber and the quality of

(a)

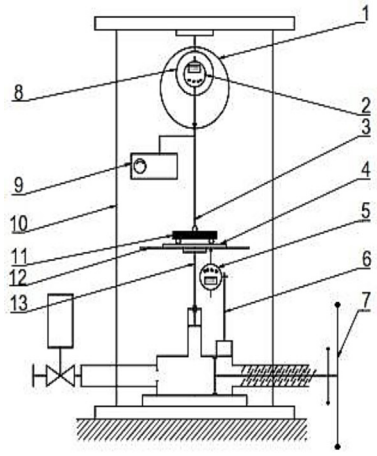

(b)

Nomenclature:
1- Buildings
2- Digital comparator
3- Strainer
4- Fixed supports
5- Digital comparator
6- Lever dial indicator support
7- Lever
8- Elastic ring
9- Lever rotation speed indicator
10- Stiffening bar
11- Sample

Fig. 4. Machine used for the bending test: (a) image of bending machine, (b) principe scheme of machine.

the weave. In order to compare the result of the modeling with that of the experimental work. The modeling of the woven is conditioned by the prior modeling of the fibers. For this, the following hypotheses have been considered:
– The friction between fibers has not been considered.
– The section of the fiber (s) is supposed to be elliptical and uniform over the length. His expression is giving by equation (10), proposed by [8]:

$$s = R_1 * R_2 * \pi, \tag{10}$$

where R_1 and R_2 are respectively large and small radius of the ellipse.
–The large radius of the ellipse is considered to be the double of small radius. The equations (11) and (12) give the expressions of the radius.

$$R_1 = 2R_2, \tag{11}$$

$$R_2 = \sqrt{\frac{S}{2\pi}}. \tag{12}$$

The application of these equations is done according to the value of the fiber section obtained experimentally by [31]. The values are given in the interval [1049; 1.90 mm^2]. They have an average of 14 745 mm^2. Therefore $R_2 = 0.484554$mm and $R_1 = 0.9691$mm.

Following the modeling of the fiber, we present in Figure 5 the modeling of the canvas starting from Pierce's empirical model.

Using the expression of moments of force of the fundamental principle of statics (PFS) at point (0) in the center of the fiber section, and neglecting the work done of the fiber weight because of its low density [0.11; 0.35 g/cm^3] [31]. The moment of the pulling force is given by

$$M_0\left(\vec{F}\right) = \left[\frac{(E_t \epsilon_t S_t)}{5N_{tr,ch}}\right].\left(\frac{d}{2}\right), \tag{13}$$

where E_t Young's modulus of the woven, ε_t deformation of the woven, S_t section of the woven $5N_{tr,ch}$, number of fibers per centimeter in the woven direction weft and chain and small diameter of the ellipse. The moment of the reaction of

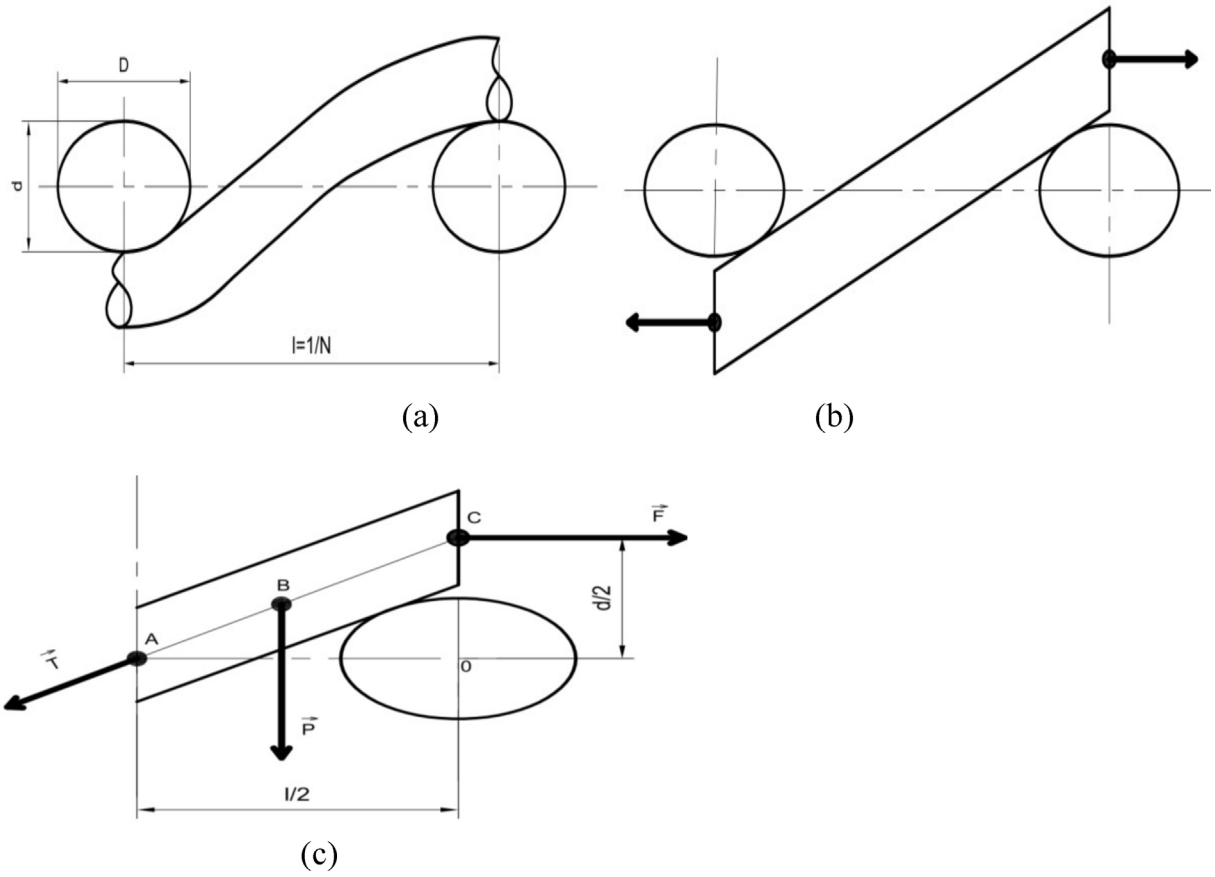

Fig. 5. Geometric modeling process of the plain weave in tensile test: (a) Pierce's geometric model [30], (b) proposed geometric model, (c) right symmetric section of (b).

the fiber is given by 14

$$M_0\left(\vec{T}\right) = \left[E_f \epsilon_f S_f . \frac{1}{2\sqrt{(d^2/4) + \left(\frac{1}{4N_{tr,ch}^2}\right)}}\right] . \left(\frac{1}{2N_{tr,ch}}\right), \quad (14)$$

where E_f Young's modulus of fiber, ε_f deformation of the fiber, S_f section of the fiber. The fundamental principle of static leads to

$$\left[\frac{(E_t \varepsilon_t S_t)}{5N_{tr,ch}}\right] . \left(\frac{d}{2}\right) - \left[E_f \varepsilon_f S_f . \frac{d}{2\sqrt{(d^2/4) + \left(\frac{1}{4N_{tr,ch}^2}\right)}}\right] . \left(\frac{1}{2N_{tr,ch}}\right) = 0. \quad (15)$$

Beyond the Young's modulus of the woven is obtained by

$$E_t = \frac{5E_f S_f \cdot \varepsilon_f}{\varepsilon_t S_t \sqrt{d^2 + \frac{1}{N_{tr,ch}^2}}}. \quad (16)$$

The expression of the deformation of the fiber is given by the derivative of the equation of the fiber tracing

$$y_f(x) = \mathrm{dcos}\left(\frac{N_{tr,ch}}{dN_{tr,ch} + 1}\pi \cdot x\right), \quad (17)$$

from the equation of the trajectory of the fiber in a woven [32]

$$z(x) = \frac{h_w + h_f}{2}\cos\left(\frac{2}{a_f + 2c_l}\pi x\right), \quad (18)$$

where π is taken as 3.14 and x is the position of a point of the woven in a given moment. Therefore

$$\varepsilon_f = \frac{\partial y_f(x)}{\partial x} . \left(\frac{1}{5N_{tr,ch}\sqrt{d^2 + \frac{1}{N_{tr,ch}^2}}}\right). \quad (19)$$

And the deformation of the woven is obtained by the derivative of the equation of the trajectory

$$y_t(x) = vx, \quad (20)$$

Table 2. Prediction equations used for optimization.

Models	Equations	
Halpin/Tsai	$E_C = E_m\left(\frac{\xi E_m(1-V_f)+E_f(1+\xi V_f)}{E_m(\xi+V_f)+E_f(1-V_f)}\right)$	(25)
Hashin	$E_C = E_f V_f + (1-V_f)E_m$	(26)
Chamis	$E_C = \frac{E_m}{1-\left(\frac{1-E_m}{E_f}\right)*sqrtV_f}$	(27)
Osoka	$E_c = E_m \sin\left(\frac{3\pi}{2}V_f^{\frac{11}{16}}\right)\left[\left(\frac{1+\xi V_f\left(\frac{E_f-E_m}{E_f+\xi E_m}\right)}{1-V_f\left(\frac{E_f-E_m}{E_f+\xi E_m}\right)}\right)\right]$	(28)
Law of mixing model series same constraint.	$E_C = E_m E_f/(E_f(1-V_f)+V_f E_m)$	(29)

Table 3. Set data for equation parameters.

	(Young's modulus of fiber)	(Young's modulus of resin)		(Fiber volume fraction)	(Reinforcement criterion) [24] With L: length of the fiber, D: diameter of the fiber
Value	4.4 GPa	3.1 GPa in traction	2.9 GPa in bending	[0; 1]	[0; 1]

with v: rest speed.

Therefore,

$$\varepsilon_t = \frac{\partial y_t(x)}{\partial x}.\left(\frac{1}{5N_{tr,ch}}\right). \tag{21}$$

The ratio between the deformation of the fiber and that of the woven fabric is

$$\frac{\varepsilon_f}{\varepsilon_t} = \frac{dN_{tr,ch}}{v(dN_{tr,ch}+1)\sqrt{d^2+\frac{1}{N_{tr,ch}^2}}}. \tag{22}$$

This allows the complete writing of the young's modulus of the woven according to its geometry and the properties of the fiber:

$$E_t = \frac{5E_f S_f d\pi N_{tr,ch}}{S_t v(dN_{tr,ch}+1)\left(d^2+\frac{1}{N_{tr,ch}^2}\right)}. \tag{23}$$

The distance between the consecutive fibers ($N_{tr,ch}$) and the young's modulus of fiber (E_f) are used to draw the curve of the solution surface giving the Young's modulus of the woven. The curve of the solution

$$E_t = f(N_{tr,ch}; E_f), \tag{24}$$

is plotted in Matlab R 2015.

2.3.2 Composite optimization

Optimization is done by the top-down gradient method applied to composite material prediction equations. In order to find the values of (volume ratio of fibre) and (reinforcement criterion) to have the largest young's module. The term optimization is used in the sense of minimization of the objective function (prediction equation).

The optimization assumptions are as follows:

- The material is assumed to be symmetrical plane and the weft reinforcement rate is the same as the warp.
- Prediction equations are continuous real variable.
- Prediction equations are differentiable and derivatives have solutions.
- Prediction equations are deterministic (the parameters and nature of the variables are known).

The mathematical function (prediction equation) associated with the problem is maximized using a simple transformation

$$\max_{V_f,\xi} E(V_f,\xi) \Leftrightarrow \min_{V_f,\xi}(-E(V_f,\xi)). \tag{30}$$

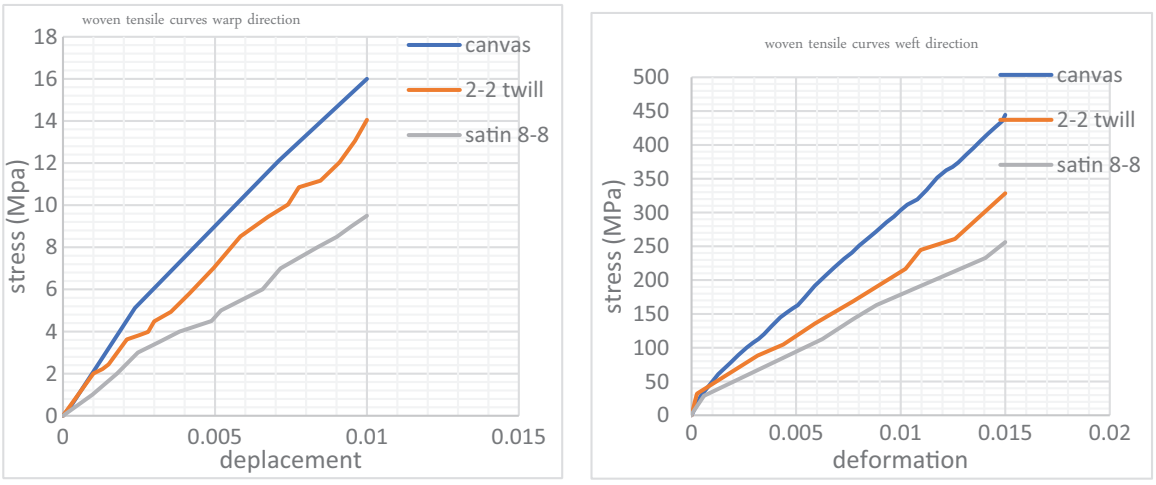

Fig. 6. Experimental tensile curves of plain fabric, twill and satin in both directions (warp and weft).

Young's modulus is optimal with the values of V_f, ξ that cancels its gradient $g(V_f, \xi)$ (Tabs. 2 and 3).

$$g(V_f,\xi) = \begin{pmatrix} \dfrac{\partial E(V_f,\xi)}{\partial V_f} \\ \dfrac{\partial E(V_f,\xi)}{\partial \xi} \end{pmatrix}. \tag{31}$$

It is therefore a question of finding the values of V_f, ξ solutions of equations

$$\frac{\partial E(V_f,\xi)}{\partial V_f} = 0. \tag{32}$$

$$\frac{\partial E(V_f,\xi)}{\partial \xi} = 0. \tag{33}$$

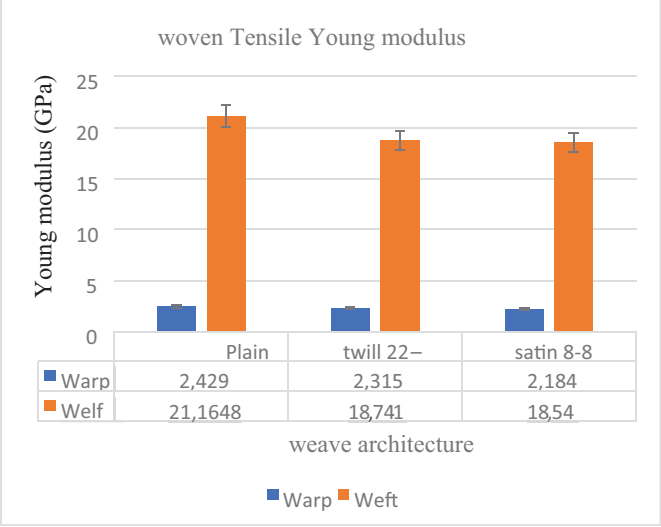

Fig. 7. Comparative diagram of the values of young's modules of the different woven armors (warp and weft direction).

3 Results and discussions

3.1 Experimental work

3.1.1 Traction of the woven fabric

The overall tensile stress behavior of different samples is the same. The samples support the gradual loading until the rupture of the first fiber when the value of the force falls. For this reason, the analysis of the experimental curve is done only before the rupture of the first fiber. The analysis of the experimental points allows us to obtain the graphs of the curves of Figure 6, representing the evolution of the deformation as a function of the imposed stress. The appearance of these curves is similar to that of previous work on waves; In the tensile characterization of fabrics made of cotton and synthetic fibers, woven according to canvas, twill and satin architectures [60] shows in this study that the canvas armor has the largest young's modulus in traction and that young's modulus is higher in the weft direction. Figure 7 showing the comparison of young's modules of the elaborated woven, presents the same result.

From the three architectures produced, the plain weave is the one with the best young's modulus, in both directions of the woven fabric (weft and warp). It is followed by the Twill and Satin weaves respectively. The difference between the weft and warp young modulus in canvas, twill and satin architectures shows that the woven young's modulus varies considerably with the number of fibers per centimeter (count/warp, weft). Knowing that the young's modulus of the raffia fiber along the rod varies in the interval [0.88; 7 GPa] [15], we find that for all woven weaves the moduli of Young in the directions have values within the range of the young's modulus of the fiber in proportion to the number of fibers used. The work of [33] on the tensile modeling of reinforced composites woven of Kenaf fibers in plain weave, twill and satin in the Wise tex software gives the same classification on the stiffness of composites according to the architecture reinforcement used; The most rigid is the canvas followed by twill and satin respectively.

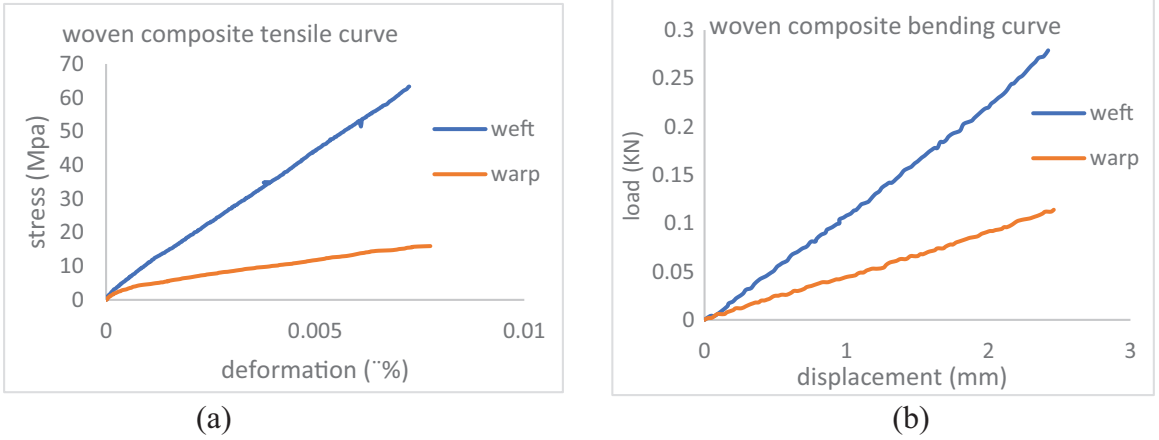

Fig. 8. Curves of the tests on the composite: (a) tensile, (b) bending.

In addition, the work of [34] on bio-composite materials reinforced with vegetable fibers shows that beyond the rigidity, the choice of the weaving weave of the material can take into account other factors, such as flexibility and permeability; Thus, depending on the application to choose, it may be possible to choose a weave other than canvas. To our knowledge, this work is the first to focus on the comparison of 2D woven reinforcement architectures experimentally using identical plant fibers.

3.1.2 Traction and bending of the composite

The armor used to reinforce the composite is the canvas armor since it has the largest Young's module. Figure 8 shows the curves of the tensile and bending tests of the composite. It shows that the composite is stiffer in the frame direction for both tests.

The bending and tensile tests carried out on the samples of composite reinforced with woven raffia fibers, show an elastic behavior of the material. This behavior is observed both for the bending test and for the tensile test and also in the two directions of reinforcement (weft and warp). The difference lies in the maximum load because there are more fibers in the weft direction than in the warp direction. Figure 8 shows the maximum stresses for the tensile test and the maximum forces for the bending test, respectively. The flexural breaking force is 28N in the weft direction and 12 N in the warp direction, weft stresses of 233.33 MPa and chain of 100 MPa. The tensile stress at break is 70 MPa in the weft direction and 20 MPa in the warp direction. These results show that the rate of reinforcement of the fibers considerably improves the ductility and toughness of the material. The Jute / Epoxy bio-composite of [35] subjected to a tensile force presents a similar shape of the curve but with a difference of the values of breaking forces in traction and in bending (43 and 55.8 MPa) of which in turn to the quality of the son. Like jute/epoxy, the bio-composite produced by [5] having for reinforcement the fiber of the palm of the Datier and the epoxy resin has a similar curve. Also, the work on the tensile strength of the bio-composite with unidirectional flax/epoxy reinforcement from [36] presents a high tensile stress. The bio-composite reinforced with pineapple leaf fibers produced by [37] also exhibits the same behavior with appreciable tensile stress. Fragassa et al. [38] present composites reinforced with woven plant fibers subjected to a tensile test the curves have the same appearance but this time showing the influence of the number of threads per centimeter (warp count and weft count) varying according to the type of febres used (Tab. 4).

In addition, by comparing Young's bending modules to those of traction in the diagram in Figure 9, we find that although the composite is more resistant in bending it is stiffer in traction. This same phenomenon is observed on the woven composite of Flax-epoxy fiber [52]. Moreover, the aforementioned works have applied in the fields of boating, automotive and aeronautics. Given the comparison between the results of this work and the latter, the woven composite of raffia epoxy fibers can be used in the same fields.

Young's modules of other composites based on natural woven fibers reinforcing epoxy resin are presented in Table 5.

This table shows the influence of the young's modulus of the fiber on the young's modulus of the composite, as shown by the work of Shah (2019) on the comparison of young's modules of plant fibers, the composites with the highest young's modules are those with the highest young's modulus of the fiber at the base.

Like several works on the study of the influence of the reinforcement rate on composites, this work evaluates the influence of the reinforcement rate of the woven fabric on the mechanical properties of the composite. Kenaf hybrid woven fiber carbon, carbon epoxy composite from [56] has a higher Young's modulus than resin cast without reinforcement when the reinforcement rate reaches 50% by volume of the composite. Likewise, the hybrid woven sisal, jute/epoxy composite from [40] shows that at 50% the tensile strength of the composite is greater than that of the moulded resin alone. Compared to other composite with woven reinforcement of vegetable fiber mixed with epoxy resin, the composite produced exhibits young's moduli in tension superior to those of the banana/epoxy, bamboo/epoxy, itles/epoxy composites; and in bending greater than banana/epoxy, bamboo/epoxy. This composite has

Table 4. Stress to the rupture of some composites reinforced with natural fibers [39].

Composite	Tensile fracture stress (MPa)	Bending fracture stress (MPa)	References
Coir−epoxy	23.68	46.63	[40]
Sisal−epoxy	37.4	52.8	
Jute−epoxy	43	55.8	[41]
Banana−epoxy	59	76.53	[42]
Bagasse−epoxy	42.4	56.7	[43]
Flax−epoxy	59.85	75.4	[44]
Areca−epoxy	27.5	25	[45]
Ramie−epoxy	90	110	[46]
Lantana Camara−epoxy	19.08	55.45	[47]
Groundnut−epoxy shell	18.09	28	[48]
Rice−epoxy shell	23	29	[49]
Coconut−epoxy	9	23	[50]
Luffa−epoxy	39.31	58.95	[51]

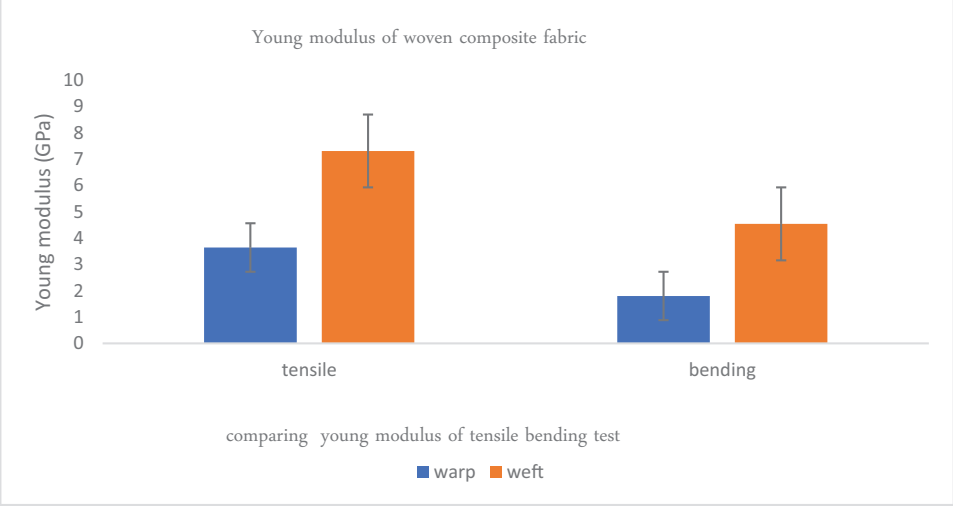

Fig. 9. Comparative distribution of young's modules in traction and bending.

young's moduli in tension (3655; 7.31 GPa) higher than that of *R. vinifiera*/polyester (1.47 GPa) with random architecture produced by [58] despite the treatment it brings to the fibers. Similarly, the composite with woven reinforcement of raffia fiber produced by [59] has slightly lower tensile performance than that achieved in this work, despite the multiple treatments carried out on the fiber to improve its adhesion with the matrix. Thus, this work shows that the best way to optimize the mechanical performance of a bio-composite with vegetable fibers in tension and in bending, consists in finding the best possible reinforcement structure (biaxial woven fabric) and associating it with a resin. Because of all the composites made with raffia fiber, the one produced in this work has the best tensile and flexural properties despite the fact that the fibers have not undergone any treatment and that the samples were produced by the contact moulding.

3.2 Theoretical results

3.2.1 Geometric modeling of canvas armor

The results of experimental tests showed plain weave as the one with the best young's modulus. Therefore, the equation (Eq. (23)) enables to assess its young's modulus as a function of it counts (warps and weft) and of the young's modulus of the raffia fiber. The equation obtained results from the modeling of the fiber and the geometry of the plain weave following a modification of the empirical geometric model of PIERCE. Like the proposed model, several empirical models describing the canvas are based on the fundamental principle of statics. But they all lead to the determination of the deformation of the woven fabric as a function of the applied load. For example, Olofson's model which introduces the shape coefficient of the yarn to develop the differential equation of the woven fabric

Table 5. Young's modulus in traction and bending of some natural fibers woven in canvas armor with epoxy as resin.

References	Composite	Young's modulus in traction (GPa)		Young's Modulus in flexion (GPa)	
		Warp	Weft	Warp	Weft
[52]	Flax−epoxy	6,385	6,254	6,183	5.62
[44]	Flax−epoxy	4,386	5.87	1,883	2,136
[29]	Hemp−epoxy	6	6	4.3	4.3
[53]	Banana−epoxy	1.9	1.9	1.85	1.85
[54]	Bamboo, E-glass/epoxy	2.49	2.49	1.75	1.75
	Henequen/epoxy	4.3	4.3	5.5	5.5
[55]	Ixtles/epoxy	3.1	3.1	4.1	4.1
	Jute/epoxy	6	6	4.5	4.5
[56]	Kenaf, carbon/epoxy	4.21	4.21	29.77	29.77
[57]	Ramie/epoxy	9.56	9.56	8.7	8.7

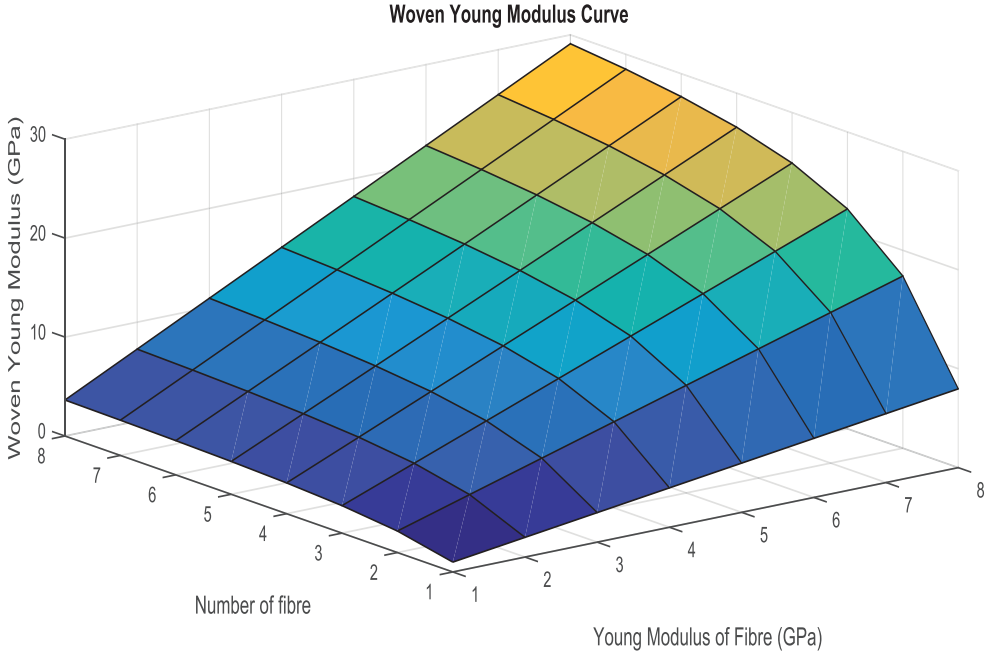

Fig. 10. Curve of the geometric modeling of the woven armor canvas.

subjected to a tensile test; the solutions are elliptical integral; Kawabata's model on the biaxial tension of the woven leads to heavy and complex equations. These different empirical models do not take into account the young's modulus of the starting fiber. And currently requires the use of software for their use. However, the equation obtained by the present modeling is to our knowledge the first which directly gives the young's modulus of the woven fabric as a function of the young's modulus of the fiber and of the geometry of the fabric. In addition, the resulting equation can be exploited using rudimentary means (small scientific calculators). Figure 10 is the representation of the solution of the modeling equation.

The theoretical young's modulus of the model for the warp count of two fibers per centimeter varies in the interval [2091; 16.63 GPa] yet the young's modulus of two fibers varies in the interval [1.76; 14 GPa]. This shows that weaving the fibers increases the rigidity of the woven. The value of the experimental young's modulus being 2429 GPa is included in the range of solution values. Similarly, the theoretical young's modulus of the model for the weft count of six fibers per centimeter varies from [3326; 26 459 GPa] when the experimental young's modulus is 21 164 GPa. The experimental results are included in the range of the solution surfaces of the theoretical model. Similarly, the theoretical model makes it possible to find young's modulus of the cotton fiber-based canvas armor woven made by [60] with a relative error of 4846%. In addition, the theoretical model applied to Kenaf's fiber which the young's modulus is given by [61] gives a result close to that obtained by [33] on the modeling of the Kenaf fiber-based composite. This

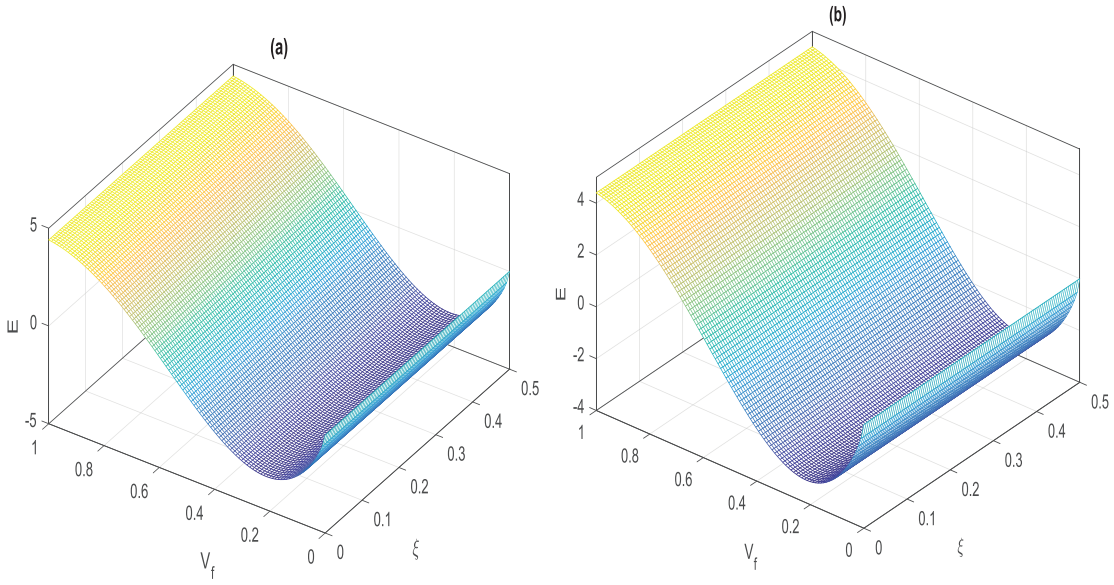

Fig. 11. Young's modulus of the composite by the Osoka model with the Young's modulus of the epoxy resin considered at 0, with $E_f = 4.4$GPa and for (a) $E_m = 3.1$GPa and (b) $E_m = 2.9$GPa.

model is thus a mathematical tool to help to determine the Young's modulus of fabrics. The simplicity of the equation allows easy and universal use.

3.2.2 Optimizations of the Young's modulus of the material by the gradient method

From the predicting equations used, only the Osoka and Halpin/Tsai models respect the imposed optimization assumptions.

3.2.3 Osoka model optimization result

The deformation gradients of the Osoka model are presented by equation (34) for the reinforcement volume fraction and equation (35) for the reinforcement criterion.

See equation (34) below.

$$\frac{\partial E(V_f,\xi)}{\partial \xi} = E_m \frac{(1-V_f)(E_f-E_m)^2 V_f \sin\left(\frac{3\pi}{2} V_f^{\frac{11}{16}}\right)}{\left(E_f+\xi E_m+(E_m-E_f)V_f\right)^2}. \tag{35}$$

The solutions of the equations (Eqs. (34) and (35)) are $V_{f0} = 0$ and, $V_{f2} = 1$, $V_{f2} = 0.25$.

Figure 11 shows the plot of the Osoka model for the Young's modulus values of resin in traction (3.1 GPa) and bending (2.9 GPa).

Among the solutions obtained shown in Figure 11, $V_{f1} = 1$ represents the material at 100% reinforcements; this solution although it is a mathematical solution is not a physical solution because this percentage represents a woven and not a composite. The value of $V_{f1} = 0$ represents a composite plate moulded without reinforcement, nor can this value be considered as a physical solution. The solution $V_{f2} = 0.25$ represents the lowest peak of the surface curve it is the only solution obtained by optimization.

The curve in the Figure 11 shows that it is not a solution of Young's modulus optimization. The reinforcement rate is the major factor influencing the evolution of the Young's modulus of the composite produced. The curve in the Figure 11 indicates that the Young's modulus of the fiber is decreasing for reinforcement rates between [0% and 25%] and increasing by [25% to 100%]; the respective real Young's moduli corresponding to these intervals are: [3.1; 1.1 GPa] and [1.1; 7.4 GPa]. The reinforcement rates from which the Young's modulus of the composite is improved are between [50%; 100%] with a corresponding Young's modulus of [3.2; 7.4 GPa]. A superposition of the curves of the cases, and shows that the extremum is independent of E_m and E_f therefore, this study is valid for all other woven composite of long vegetable fibers. Although the fiber matrix adhesion is an important parameter on the Young's modulus of the raffia/polyester fiber composite [21], and of the woven raffia/polyester fiber [59] its influence does not have a measurable direct impact on the Young's modulus of the woven raffia /epoxy fiber composite in view of the plot of the

$$\frac{\partial E(V_f,\xi)}{\partial V_f} = E_m \left(\frac{33}{32}\pi \frac{(E_f+\xi E_m+\xi V_f(E_f-E_m))\cos\left(\frac{3\pi}{2} V_f^{\frac{11}{16}}\right)}{(E_f+\xi E_m+(E_m-E_f)V_f)V_f^{\frac{5}{16}}} + \frac{(1+\xi)(E_f+\xi E_m)(E_f-E_m)\sin\left(\frac{3\pi}{2} V_f^{\frac{11}{16}}\right)}{(E_f+\xi E_m+(E_m-E_f)V_f)^2} \right), \tag{34}$$

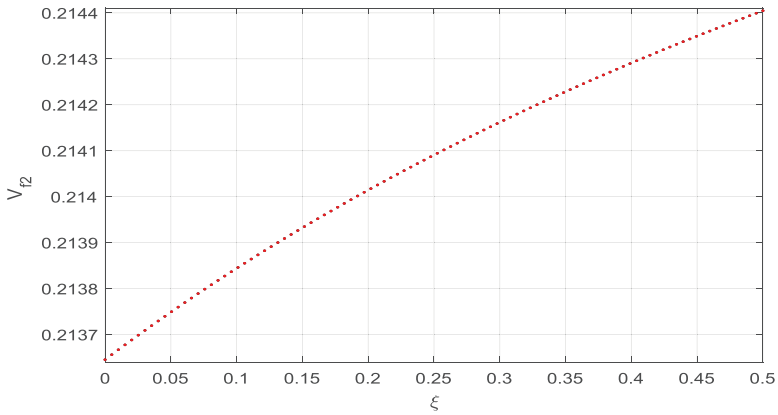

Fig. 12. Evolution of V_f as a function of ξ.

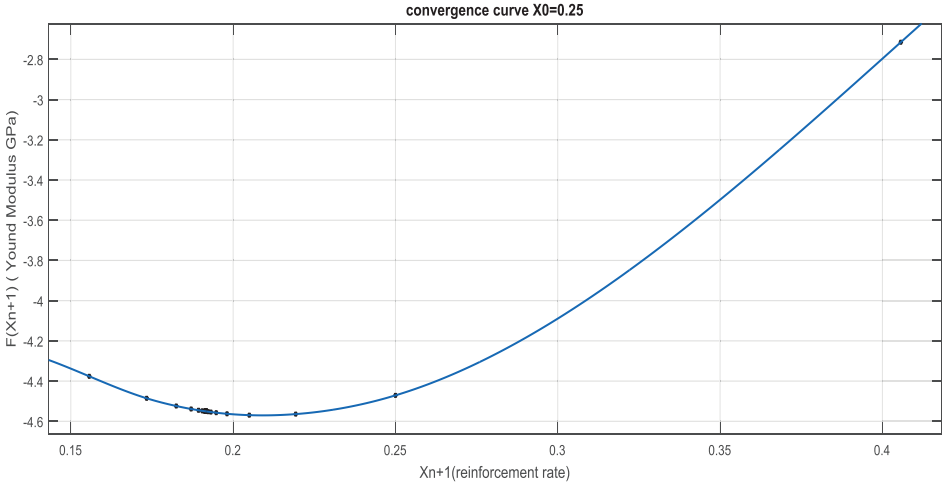

Fig. 13. Convergences curves for descend gradient analysis method.

Osoka model. However, its impact on the reinforcement rate is perceptible. The curve in the Figure 12 is an illustration of this impact.

In view of the result presented by the curve Figure 13, it is important and necessary to study the convergence of the solution. In order to precisely find the point of minimization. Considering the fact that the reinforcement criterion and young modulus does not directly influence the result, they are been taken constant at a value of $\xi = 0.5$ and $E = 3.1$ GPa. To find the minimize point, descend gradient algorithm has been applied [62] to Osoka equation (Eq. (28)). Descent gradient analysis consider the initial point $X_0 = 0.25$ and the convergence rate $\alpha = 0.01$.

The analysis has been done from 200 iterative points. The global minimize point has been given by $X_m = 0.2192$ after four iterations. Thus, the rate of reinforcement which minimizes the young modulus is 21.92%.

Osoka's model of prediction on the Young's modulus of the composite produced allows to have for the theoretical reinforcement rates of 20% and 60%, the respective young modulus of 1.3 GPa and 4.5 GPa. Thus, the theoretical Young's modulus approaches with a relative difference of 2% from the experimental one.

3.2.4 Optimization result of the Alpin/Tsai, Hashin, Chamis, mixing law model

The gradient equations of the Halpin/Tsai model are presented by equations (36) and (37):

See equation (36),(37) below.

$$\frac{\partial E(V_f,\xi)}{\partial V_f} = E_m\left[\frac{(\xi E_m + \xi E_f)\left(\left(E_m(\xi+V_f)\right)+E_f(1-V_f)\right) - \left(\left(E_m-E_f\right)\left(\xi E_m(1-V_f)+E_f(1+\xi V_f)\right)\right)}{\left(\left(E_m(\xi+V_f)\right)+E_f(1-V_f)\right)^2}\right], \quad (36)$$

$$\frac{\partial E(V_f,\xi)}{\partial \xi} = E_m\left[\frac{E_m(1-V_f)\left(\left(E_m(\xi+V_f)\right)+E_f(1-V_f)\right) - \left(E_m\left(\xi E_m(1-V_f)+E_f(1+\xi V_f)\right)\right)}{\left(\left(E_m(\xi+V_f)\right)+E_f(1-V_f)\right)^2}\right]. \quad (37)$$

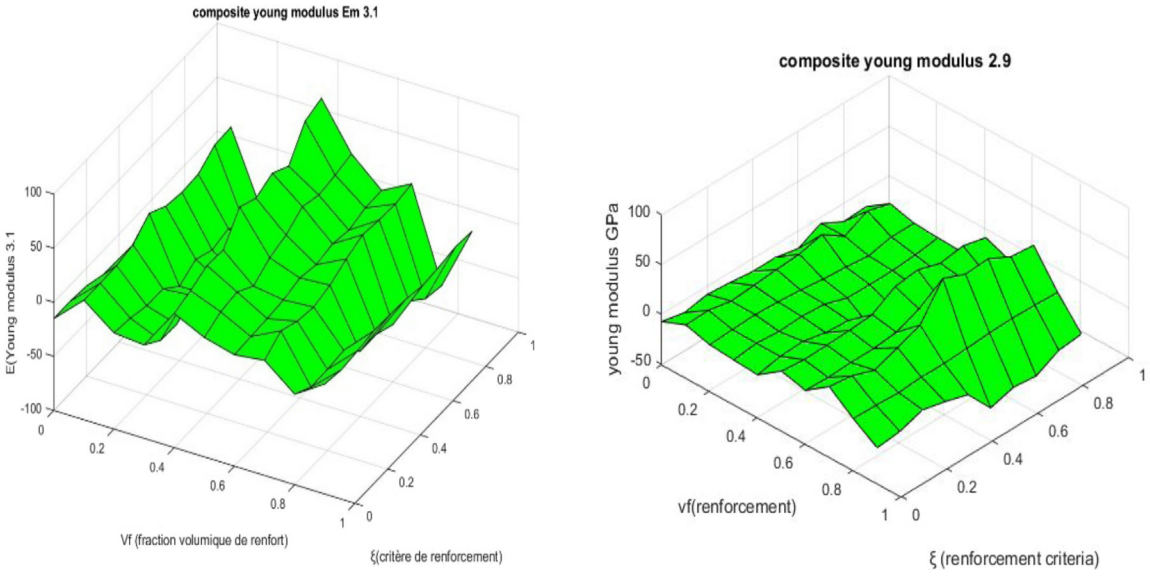

Fig. 14. Surface solutions of the Alpin Tsai model.

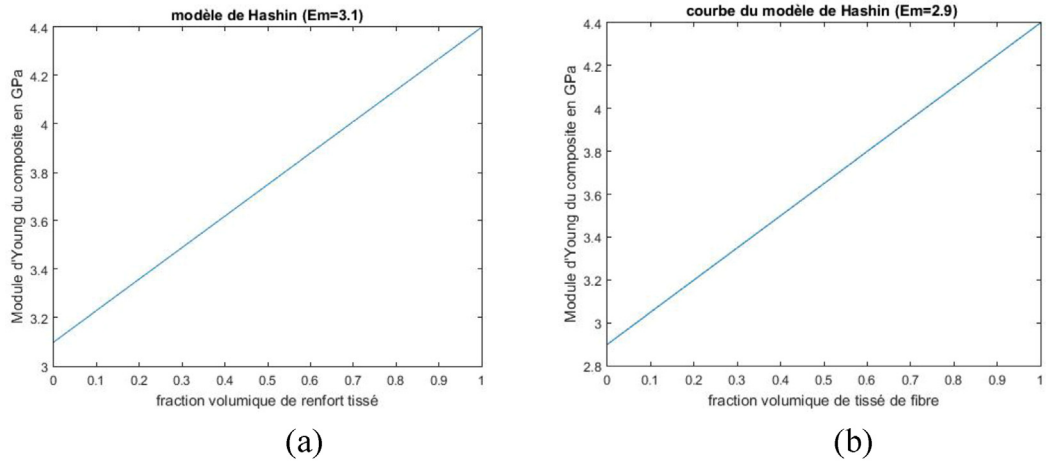

Fig. 15. Hashin model: (a) tensile, (b) flexural.

The equations (36) and (37) present solutions that we can perceive through the plot of the Halpin/Tsai model in the Figure 14. The images of the solutions of the Alpin/Tsai model do not correspond to the result of the experimental work. This model therefore does not correspond to the composite produced. Moreover, unlike the Osoka model, the plot of the Halpin/Tsai model presents solutions according to the reinforcement criterion. The shape of the curve changes depending on the Young's modulus of the resin.

Although the models of Chamis, Hashin and that of the law of mixtures do not respect the optimization assumptions, the curves corresponding to the material parameters have been drawn for these different models are represented in Figures 15−17.

These three models show overall that the Young's modulus of the woven fabric increases with the reinforcement rate from 0% to 100%. However the results of the experimental work show that at 20% of the reinforcement rate, the Young's modulus of the composite in bending (1802 GPa) is less than that of the resin. In addition, the theoretical maximum Young's modulus that can be envisaged is 4.4 GPa but the experimental work gives a maximum Young's modulus of 7.31GPa in tension and 4.54 GPa in bending.

From the different prediction models used, Osoka's model is the best and the most appropriate. It is also recommended having a reinforcement rate >50% to significant improve the rigidity of the resin.

4 Conclusion

This work focused on optimizing the Young's modulus of the composite reinforced by the woven raffia fiber. It was done experimentally and theoretically on the woven and the composite material. The comparison of Young's moduli according to the weave, and the number of fibers per centimeters of canvas, twill and satin armor, experimentally shows that the canvas weave gives the highest Young's

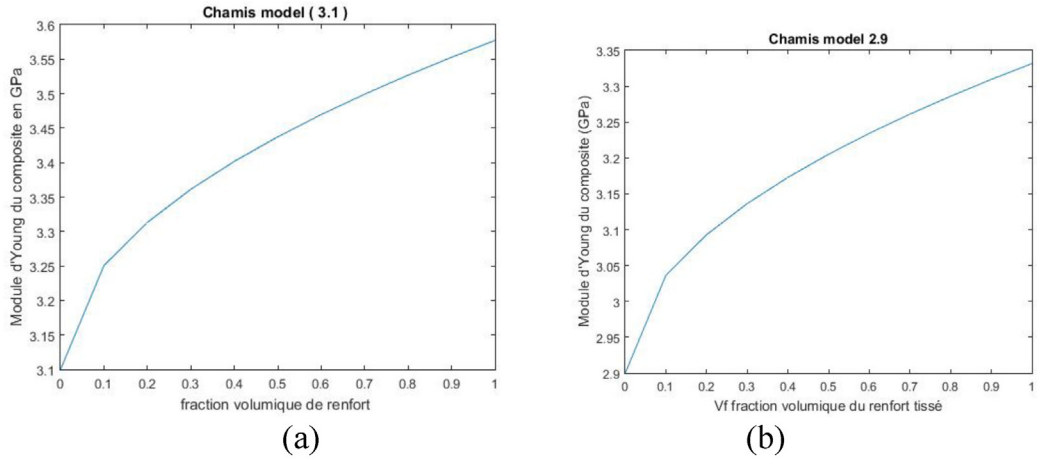

Fig. 16. Chamis model curve: (a) tensile test, (b) flexural test.

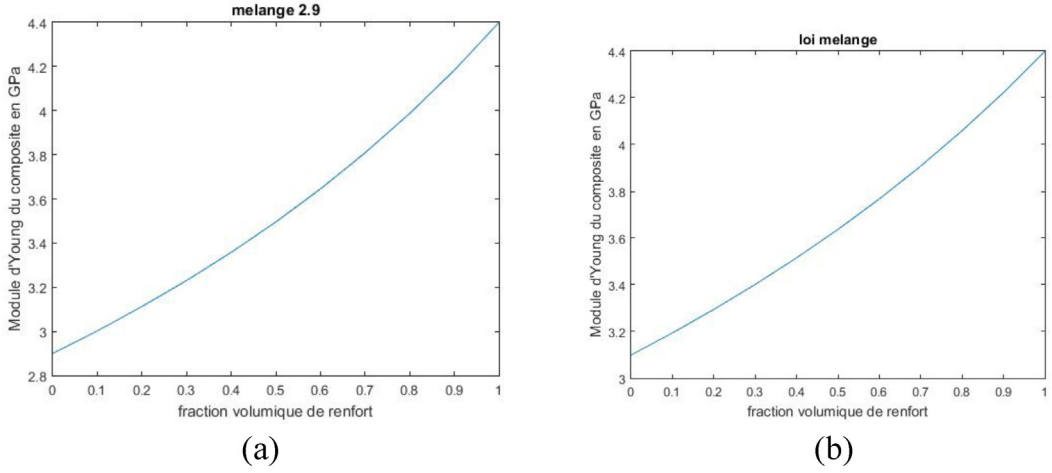

Fig. 17. Mixing law: (a) in bending tests, (b) tensile test.

modulus followed by twill and satin respectively. And that the Young's modulus of the woven fabric increases significantly with the number of fibers and interweaving between the fibers. The geometrical modeling of the canvas woven fabric permits to establish the equation which shows the evolution of the Young's modulus of the woven fabric as a function of the number of fiber. The mathematical result corroborates with the results obtained experimentally, and reveal that the woven fabric can be used to reinforce resin, and as a decoration tool because of their aesthetic appearance. The composite reinforces with canvas woven has been characterized in tensile and bending test. The values of the young's moduli obtained from tensile and bending test in both warp and weft directions are closed to other bio-composites and mainly depends on the reinforcement structure. Having studied the optimization of the composite young's modulus, the prediction model of Osoka best suit the experimental results and the reinforcement rate as from 50% upward contribute to strengthen the composite material. The optimization work also shows that the parameter which takes into account the fiber matrix interphases, fiber alignment problems does not directly influence the Young's modulus of the composite but rather the volume fraction. This composite material can be used in the automotive and nautical industries for interior trim, dashboards and compartments.

Conflict of Interests

The authors declare that is no conflict of interest regarding the publication of interests regarding the publication of this paper. All this research work has been funded from own funds.

References

1. ISO, Textiles-tensile properties of fabrics, part 1: determination of maximum force and elongation at maximum force using the strip method, 2013
2. D. Norm, En ISO 527-5, no. 1108 1997
3. British Standards Institution, BS EN ISO 14125:1998 Licensed, A.J. Order, Theory Ordered Sets Its Appl., vol. 1998, July 2002, p. 24, 1998 [Online]. Available at: https://books.google.com/books?id=JZBNMwEACAAJ&pgis=1

4. A. Hallonet, Développement et caractérisation d'un matériau composite à base de fibres de lin: application au renforcement de structures en béton par collage externe, PhD thèse, Univ. Lyon, p. 231, 2016
5. T. Djoudi et al., Physico-mechanical characterization of composite materials based on date palm tree fibers, J. Nat. Fibers **18**, 789–802 (2021)
6. T.T. Stanislas et al., Production and characterization of pulp and nanofibrillated cellulose from selected tropical plants, J. Nat. Fibers **19**, 1592–1608 (2020)
7. L. Gornet, materiaux composites to cite this version: généralités sur les matériaux composites, pp. 1–48, 2011.
8. G.B. Hughes, Calculating ellipse overlap areas, March 2018
9. B. Beckelynck, Étude de la délamination sur des matériaux composites tissés taffetas: essais de caractérisation et simulations numériques, 2016
10. R. Muñoz Sánchez, Mechanical behavior of hybrid 3D woven composites, doctoral thesis, p. 228, 2014
11. E.H. Taibi, Caracterisation, modélisation et simulation du comportemet d'un tissu textile, 2001
12. J. Vilfayeau, Modélisation numérique du procédé de tissage des renforts fibreux pour matériaux composites, Comptes Rendus des JNC 18, 2013.
13. L.P. Brown et al., Characterisation and modelling of complex textile geometries using TexGen, IOP Conf. Ser. Mater. Sci. Eng. 406 (2018). doi: 10.1088/1757-899X/406/1/012024
14. S. Wahab et al., Analysis of mechanical properties for 2D woven kenaf composite analysis of mechanical properties for 2D woven kenaf composite, October 2018, 2014, doi: 10.4028/www.scientific.net/AMM.660.125
15. S. Tagne Nicodème Rodrigue et al., Investigation of the physical and mechanical properties of Raffia vinifera fibers along the stem, J. Nat. Fibers **14**, 621–633 (2017)
16. Ship Structure Committee, Design Guide for Marine, 1997
17. J. Luc, Optimisation des propriétés mécaniques de composites à base de fibres naturelles: application à un composite de fibre de lin avec un mélange de polyéthylène/polypropylène d'origine post-consommation, 2015
18. A. Ghosh et al., Optimization of knitted fabric comfort and UV protection using desirability function, J. Eng. Fiber. Fabr. **11**, 20–28 (2016)
19. B. Zuccarello et al., New concept in bioderived composites: biochar as toughening agent for improving performances and durability of agave-based epoxy biocomposites, Polymers (Basel) **13**, 1–14 (2021)
20. A. Majumdar et al., Optimization of woven fabric parameters for ultraviolet radiation protection and comfort using artificial neural network and genetic algorithm, Neural Comput. Appl. **27**, 2567–2576 (2016)
21. E.G. de O. Filho et al., Effect of chemical treatment and length of raffia fiber (Raphia vinifera) on mechanical stiffening of polyester composites, Polymers (Basel) **12**, 1–17 (2020)
22. K.K. Agarwal, G. Agarwal, A study of mechanical properties of epoxy resin in presence of a study of mechanical properties of epoxy, June, 2019
23. Z. Boufaida, Analyse des propriétés mécaniques de composites taffetas verre/matrice acrylique en relation avec les propriétés d ' adhésion des fibres sur la matrice, p. 213, 2015
24. O.D.O. Osoka Emmanuel, A modified Halpin-Tsai model for estimating the modulus of natural fiber reinforced composites, Int. J. Eng. Sci. Invent. **7**, 63–70 (2018)
25. O. Harmouzi, Matériaux lignocellulosiques fonctionnels à partir a de plantes vivaces marocaines et de pates commerciales, J. Org. Chem. 3965 (2010)
26. C. Florimond, Contribution a la modelisation mecanique du comportement de meche de renforts tisses a l'aide d'un schema elements finis implicite, 2013
27. D.S. Ivanov, S.V. Lomov, Compaction behaviour of dense sheared woven preforms: experimental observations and analytical predictions, Compos. Part A Appl. Sci. Manuf. **64**, 167–176 (2014)
28. N. Dieunedort et al., Characterization of a brake lining composite based on aiele fruit cores (Canarium schweinfurthii) and palm kernel fibers (Elaeis guineensis) with a urea-formaldehyde matrix, Int. J. Sci. Eng. Res. **11**, 1110–1117 (2020)
29. R. Sepe et al., Mechanical properties of hemp fibre/epoxy composites. Influence of fibre chemical treatments, ECCM 2016 - Proceeding 17th Eur. Conf. Compos. Mater., June, pp. 26–30, 2016
30. F.T. Peirce, Geometry of Cloth Structure, J. Text. Inst. **28**, 45-96 (1937)
31. N.R.S. Tagne et al., Physicochemical and mechanical characterization of Raffia vinifera pith physicochemical and mechanical characterization of Raffia vinifera pith, December 2020, doi: 10.1155/2020/8895913
32. M. Hung, Modélisation des architectures à renforcement tridimentionnel dans les structures composites, 2014
33. M.S. Wahab et al., Analysis of mechanical properties for 2D woven kenaf composite, Appl. Mech. Mater. **660**, 125–129 (2014)
34. H.A. Aisyah et al., A comprehensive review on advanced sustainable woven natural fibre polymer composites, February 2021, doi: 10.3390/polym13030471
35. A. Mir et al., Caractérisation mécanique et thermomécanique d'un stratifié Jute / époxy [Mechanical and thermomechanical characterization of jute/epoxy laminate], HAL hal- 0038 9086, 2009
36. G. Coroller et al., Effect of flax fibres individualisation on tensile failure of flax/epoxy unidirectional composite, Compos. Part A Appl. Sci. Manuf. **51**, 62–70 (2013)
37. A.R. Sena Neto et al., Comparative study of 12 pineapple leaf fiber varieties for use as mechanical reinforcement in polymer composites, Ind. Crops Prod. **64**, 68–78 (2015)
38. C. Fragassa, C. Fragassa, Effect of natural fibers and bio-resins on mechanical properties in hybrid and non- hybrid composites, 020118 (2019), doi: 10.1063/1.4949693
39. R. Jeyapragash et al., Mechanical properties of natural fiber/particulate reinforced epoxy composites – a review of the literature, Mater. Today Proc. **22**, 1223–1227 (2020)
40. T.K. Khieng, A review on mechanical properties of natural fibre reinforced polymer composites under various strain rates, J. Compos. Sci. **5**, 1–13 (2021)
41. M. Kumar, R. Singh, Development of the hybrid natural fiber reinforced polymer composites using the bidirectional sisal and woven jute fiber, Int. J. Tech. Res. Sci. **05**, 35–42 (2020)
42. A.P. Irawan, I.W. Sukania, Tensile strength of banana fiber reinforced epoxy composites materials, Appl. Mech. Mater. **776**, 260–263 (2015)
43. P. Dwivedi et al., Study of mechanical behaviour & water-absorption characteristics of sisal-bagasse fibre reinforced hybrid epoxy composites, Int. J. Eng. Tech. Res. **9**, 23–32 (2019)
44. C. Cerbu, Mechanical characterization of the flax/epoxy composite material, Procedia Technol. **19**, 268–275 (2015)

45. S. Dhanalakshmi et al., Areca fiber reinforced epoxy composites: effect of chemical treatments on impact strength, Orient. J. Chem. **31**, 763–769 (2015)
46. Z. Djafar et al., Tensile and bending strength analysis of ramie fiber and woven ramie reinforced epoxy composite, J. Nat. Fibers **18**, 2315–2326 (2021)
47. R.H. Rao et al., Study on mechanical behaviour of banana fiber reinforced epoxy composites, Asian J. Multidiscip. Res. **5**, 1–4 (2019)
48. A.J. Olaitan et al., Comparative assessment of mechanical properties of groundnut shell and rice husk reinforced epoxy composites, **5**, 76–86 (2017)
49. H. Salem, E. Tayeb, The impact of rice straw micro fibres reinforced epoxy composite on tensile strength and break strain, Int. J. Sci. Eng. Res. **5**, 58–62 (2014)
50. M.S.R. and S.M.S.M.M.B.H. Salleh et al., Mechanical properties of coconut carbon fibre / epoxy composite material, Int. J. Mech. Eng. **2**, 55–62 (2013)
51. D. Chakrabarti et al., Effect of chemical treatment on the mechanical properties of luffa fiber reinforced epoxy composite, J. Eng. Adv. **01**, 37–42 (2020)
52. V. Gopalan et al., Dynamic characteristics of woven flax/epoxy laminated composite plate, Polymers (Basel) **13**, 1–14 (2021)
53. M.A. Maleque et al., Mechanical properties study of pseudo-stem banana fiber reinforced epoxy composite, Arab. J. Sci. Eng. **32**, 359–364 (2007)
54. R.S., et D.S.B.Venkatesha, Mechanical properties of woven bamboo/E-glass fiber reinforced epoxy hybrid composites, Trans Stellar, 2020
55. V.R.-R., E.F.-U. Mauricio Torres-Arellano, Mechanical properties of natural-fiber-reinforced biobased epoxy resins manufactured by resin infusion process, 2020
56. N. Sarifuddin et al., Mechanical properties of woven carbon fiber/Kenaf fabric reinforced epoxy hybrid composites, 2019
57. A.P. Irawan et al., Tensile and flexural strength of ramie fiber reinforced epoxy composites for socket prosthesis application, Int. J. Mech. Mater. Eng. **6**, 46–50 (2011)
58. R.T. Fujiyama, A. Clay, Effect of chemical treatment and length of Raffi a fiber (Raphia vinifera) on mechanical stiffening of polyester composites, 2020
59. D. Kocak et al., Research into the specifications of woven composites obtained from raffia fibers pretreated using the ecological method, Text. Res. J. **85**, 302–315 (2015)
60. S. Dridi, Essais de caractérisation des structures tissées, Institut National des Siences Appliquées de Lyon, 2010
61. M.H.M. Amin et al., An evaluation of mechanical properties on kenaf natural fiber/polyester composite structures as table tennis blade, J. Phys. Conf. Ser. 914, (2017), doi: 10.1088/1742-6596/914/1/012015
62. A. Boltnev, N. Kalitkin, Speeding up the convergence of, pp. 349–354, 2005.

Cite this article as: Alfred Kendem Djoumessi, Rodrigue Nicodème Sikame Tagne, Tido Tiwa Stanislas, François Ngapgue, Ebenezer Njeugna, Optimization of the Young's modulus of woven composite material made by *Raphia vinifiera* fiber/epoxy, Int. J. Simul. Multidisci. Des. Optim. **13**, 21 (2022)